Int. J. Electrochem. Sci., 12 **(2017)** 8552 – 8563, doi: 10.20964/2017.09.60

International Journal of ELECTROCHEMICAL SCIENCE
www.electrochemsci.org

Creatine Kinase Determination Based on an Electrochemical Impedance Immunosensor

Tao Geng, Zhiyuan Song, Jiangang Zhang and Zesheng Xu[*]

The Second Department of Cangzhou Cardiovascular Institute, No.16 West Xinhua Rd, Cangzhou, Hebei, 061000, P.R. China
[*]E-mail: xuzensheng79@163.com

Received: 23 May 2017 / *Accepted:* 20 July 2017 / *Published:* 13 August 2017

With biosynthesized gold nanoparticles (Au NPs) as the basis, a new electrochemical impedance immunosensor is proposed in this study to determine the concentration of creatine kinase (CK), a cardiac biomarker. This sensor has an extended detecting range of 10 ng/mL to 0.5 μg/mL. Moreover, it features a notable anti-interference trait making this bio-fabricated immunosensor potentially employable in CK detection.

Keywords: Creatine kinase; Electrochemical impedance immunosensor; Gold nanoparticle; Acute myocardial infarction; Clinical measurement

1. INTRODUCTION

Present in the cells of human muscle (most widely observable in myocardium and skeletal muscles), creatine kinase (CK) is regarded as a significant intracellular enzyme. After the depletion of ATP storage in muscle cells during active muscular work, a phosphate is transferred from creatine phosphate to ADP by CK as a means of synthesizing new molecules of ATP. Therefore, the extra energy embodied in the creatine phosphate form is provided to the muscles by CK. The catalysis of a reverse reaction is performed by CK to create a reserve of creatine phosphate when the muscles are at rest. In the blood serum of a healthy female, a CK level of 0.026–0.14 U/ml is observed, while in that of a healthy male, the range observed is 0.038–0.174 U/ml; both ranges are rather low. In the blood serum of a child, the concentration of CK is several times larger. The CK concentration increases to as high as 2.0 U/ml or 39–185 ng/ml during manual labour and muscular injuries caused by muscular dystrophy, myocardial infarction and diverse inflammation courses [1-3]. Moreover, hypothyroidism is another situation in which an increase in CK activity is observed in the blood serum. Normally

functioning as a biomarker of acute myocardial infarction (AMI), CK concentration/activity is determined in contemporary clinical diagnosis to confirm other AMI-related symptoms. Succeeding the outbreak of AMI, there is an instant rise in CK levels in the blood, and after 4–6 h it turns unusual, with the peak value of CK activity occurring 18–24 h after the outbreak of AMI [3]. The seriousness of the AMI is assessed using the measurement of the CK rise, which determines the appropriate therapeutic action to take [4]. Furthermore, CK measurement in the blood serum is used in the evaluation of athletes' physical qualities.

CK is normally determined by medical laboratories with inexpensive and complicated spectrophotometric approaches. The production rate of the products of the CK-catalysed reaction are measured to evaluate CK activity [5, 6]. Usually, a hexokinase and glucose-6-phosphate dehydrogenase based enzymatic system is employed. CK-synthesized ATP is employed by hexokinase to synthesize glucose-6-phosphate. The formation of NADH is achieved by the oxidation of the latter with glucose-6-phosphate dehydrogenase. NADH concentration is determined through spectroscopy at 340 nm and used to calculate the activity of CK in the sample. This approach is unable to differentiate between diverse CK isoforms, with the total activity of all isoforms being measured.

Immunological techniques outperform other methods of determining the concentration of biomarkers such as CK in selectivity and precision [7]. An immunoassay is employed that detects specific CK-antibody binding that results in chemiluminescence, which can be detected through electrochemical means. [8]. The CK concentration of samples that have experienced long-term or improper storage can also be determined by this technique due to its focus on CK weight concentration (in nanograms) instead of CK activity. The ability to determine the tissue that originally released the CK is another benefit of immunological techniques. There is also the potential to separately determinate diverse CK isoforms. However, the disadvantages of this technique include the inability to repeatedly use the major reaction elements, the necessity of an animal antibody, and the high cost. Based on colorimetric analysis, chromatography, electrochemistry, spectroscopy and other signal-transduction theories, diverse immunoassays have been proposed in recent years to determine protein biomarkers [7, 9-13]. Since electrochemical detection in such techniques requires simple tools and is inexpensive and significantly sensitive, it is regarded as the preferred assay technique [14, 15]. Based on previous literature, when developing electrochemical immunoassays with desirable analytical traits, two major factors have to be considered: the fabrication of a significantly effective signal-production label, [16] and the application of a detection mode with significant sensitivity [17]. The realization of a low-grade detection limit and quantification requires the signal to be amplified sufficiently. Novel analytical instrumentation and tools can be developed by nanomaterial production, manipulation and deployment procedures, as found in the field of nanotechnology [18, 19]. In terms of stripping voltammetric detection, desirable electronic activity, simple fabrication and other inner strengths, Au nanostructures are a promising option. To achieve significantly sensitive genomic DNA detection, a hollow polyelectrolyte shell containing Au atoms (roughly 1.0×10^{11}) with favourable Au nanoparticles dispersion was employed by Khunrattanaporn and co-workers to fabricate a stripping voltammetric label [20]. Sensing DNA-oligonucleotide interactions, the complexes of avidin-biotin, antibody-antigen formation, and other biological interfaces could be achieved by measuring electrical traits with sensitivity and in a non-destructive way by electrochemical impedance spectroscopy (EIS)

[21, 22]. In this work, a bioelectrode was fabricated to detect CK with biosynthesized Au NPs utilizing the EIS technique. An indium-tin-oxide (ITO)-glass plate provides a platform for the covalent anchoring of biosynthesized Au NPs on the self-assembled monolayer (SAM) of 3-aminopropyltriethoxy silane (APTES). The carbodiimide coupling reaction contributes to the covalent attachment of Ab-CK (CK antibody) to APTES/ITO-glass plates modified by carboxyl-functionalized Au NPs. Diverse microscopic approaches were employed for a systematic characterization of the bioelectrode. Additionally, EIS ($[Fe(CN)_6]^{3-/4-}$ as a redox probe) is employed for the investigation of this bioelectrode's capacity to quantitatively estimate Ag-CK in phosphate buffer saline (PBS) with a pH of 7.4.

2. EXPERIMENTS

2.1. Chemicals

PBS containing NaCl (140 mM), KCl (2.7 mM), Na_2HPO_4(0.1 mM) and KH_2PO_4 (1.8 mM), pH 7.2 was employed in the whole set of experiments as the buffer solution. $K_3[Fe(CN)_6]/K_4[Fe(CN)_6]$ (10 mM) was added to the buffer where a redox mediator was necessary. 3-mercaptopropionic acid (MPA), bovine serum albumin, creatine kinase (CK), 2-mercaptoethylamine (2-MEA) hydrochloride and $HAuCl_4$ were purchased from Sigma-Aldrich Corp. To remove impurities, fresh *Pithophora oedogonia* was washed with Mill-Q water. The wet sample went through 3 days of shade drying, followed by a complete 70 °C oven drying. Eventually, the final Pithophora oedogonia sample was obtained as a fine powder through grounding. Being of analytical grade, the rest of the chemicals were used without further purification.

2.2. AuNPs synthesis

A mixture of water (100 mL) and *Pithophora oedogonia* powder (10 g) was sonicated for 15 min, then heated at 70 °C for 15 min to synthesize Au NPs. Filter paper with pore size of 200 nm was employed for the filtration *of Pithophora oedogonia* extract. A mixture of $HAuCl_4$ solution (20 mL) and *Pithophora oedogonia* extract (20 mL) was sonicated for 1 h to achieve the synthesis of Au nanoparticles, indicated by the solution's colour change from light yellow to purplish yellow. A 0.5 h, 10,000 rpm centrifugation and a subsequent wash cycle were performed for separation. The Au nanoparticles were then dried in an over at 70 °C. Au NPs solution stabilization was achieved by the instant addition of a mixture of H_2O (10 mL) and MPA (46 μL). 50 mL was maintained as the terminal volume of reaction mixture, which went through 2 h stirring at ambient temperature. Then, these colloidal solutions went through ethanol washing two or three times, 20000 rpm centrifugation and 12 h vacuum drying.

2.3. Characterizations

A UV-2550 spectrophotometer (SHIMADZU, Japan) was employed to obtain UV absorption spectra. X-ray diffraction (XRD) was employed to carry out the qualitative phase analysis of the electro-catalyst with the Philips XPERT PRO system. The Fourier-transform infrared spectra (FT-IR) of the samples were recorded using a Bruker Equinox 55. An ESCALab220i-XL electron spectrometer purchased from VG scientific was used to measure the X-ray photoelectron spectroscopy (XPS) data with Al Kα radiation of 300 W, where the base pressure was approximate 3×10^{-9} mbar.

2.4. Immunosensor fabrication

The glass plates coated with ITO were ultrasonically cleaned and subsequently vacuum dried. Cleaned ITO glass plates were exposed to oxygen plasma in a plasma chamber for 5 minutes to increase the hydroxyl species on the surface. Then an SAM of APTES was generated by 1.5 h immersion of ITO-glass plates into 2% APTES solution prepared in ethanol in ambient conditions. For the non-bonded APTES to be removed from the substrate surface, the plates went through ethanol rinsing. Then, N_2 gas flow drying was conducted on them. 3 h immersion of these APTES-modified ITO glass plates was performed in the as-prepared mixture of functionalized Au(MPA) nanoparticles. The immunosensor (Au(MPA)/APTES/ITO-glass) was fabricated after the following double-distilled water washing and N_2 gas flow drying. The immobilization of Ab-CK on as-prepared electrode was achieved after it went through 4 °C treatment with PBS containing 100 μg/mL Ab-CK overnight, PBS washing and N_2 flow drying (denoted as Ab-CK/Au(MPA)/APTES/ITO-glass). For the nonspecific binding sites to be impeded on the surface of the electrode, 30 min incubation of this Ab-CK-immobilized electrode was performed in the solution of BSA (1%). The electrode then went through PBS washing for the removal of any physically adsorbed antibodies, followed by N_2 flow drying.

2.5. Electrochemical determination

A triple electrode system was employed to electrochemically determine the carbendazim. In this electrode system, the roles of the counter and reference electrode were respectively taken by a Pt foil and a saturated Ag/AgCl. PBS (pH 7.4, 0.1 M KCl) solution containing 2 mM $[Fe(CN)_6]^{3-}$/$[Fe(CN)_6]^{4-}$ was used for EIS measurements at an AC voltage of 0.05 V in a frequency range of 1 Hz - 100 kHz. Equal portions of Ag-CK from the 100 μg/mL stock solution were treated in PBS with diverse concentrations. After these equal portions with diverse concentrations were successively added to the PBS solution containing 2 mM $[Fe(CN)_6]^{3-}$/$[Fe(CN)_6]^{4-}$, the measurement of the Ab-CK/Au(MPA)/APTES/ITO-glass bioelectrode was performed for its EIS response. A specimen solution in the absence of Ag-CK was used for impedance measurement, where the control specimen response was represented by its corresponding electron transfer resistance (R_{et}) shown in a Nyquist plot. To achieve the detection of the immunoreactions between the antigen and antibody, R_{et} and

relevant parameters concerning EIS were assessed after the equal portions of Ag-CK with diverse concentrations were successively added.

3. RESULTS AND DISCUSSION

As soon as *Pithophora oedogonia* extract was mixed into $HAuCl_3$ solution, the biosynthesis reaction was initiated. Au nanoparticles began nucleating, denoted by the change in the dispersion colour from the original light yellow to purplish yellow. Light at certain wavelength could be absorbed by the scattered metallic nanoparticle. In this way, in the as-prepared Au NPs dispersion, the surface plasmon resonances of the Au NPs would be monitored. Note that several elements such as size, solvent and morphology would influence the optical trait of Au NPs [23]. The *Pithophora oedogonia* prepared Au NPs were characterized via UV-vis spectrometry in Figure 1A. That the metallic Au material was formed could be verified through the surface plasmon resonance of the Au NPs represented by the 525 nm absorption peak. The mean size of the synthesized Au NPs was determined by the location of the surface plasmon resonance peak. XPS also verified the fabrication of the Au NPs. The biosynthesized Au NPs were characterized by Au_{4f} high resolution XPS scan, as indicated in Figure 1B, with 83.5 and 87.2 eV obtained respectively for $Au_{4f\ 7/2}$ and $Au_{4f\ 5/2}$ peaks. These peaks indicated a transfer from the theoretical Au^0 values of 84.0 and 87.7 eV due to the surface attachment of biomolecules coming from the *Pithophora oedogonia* extract. The biosynthesized Au NPs were characterized by an XRD profile in Figure 1C. The (311), (220), (200) and (111) planes of face-centred-cubic (fcc) crystallographic structure of Au (JCPDS 4-0783) were denoted respectively by the 81.9°, 67.7°, 45.9° and 39.3° diffraction peaks of the biosynthesized Au NPs shown in the XRD spectrum. That the metallic Au was successfully fabricated was further verified by the results of XRD analysis.

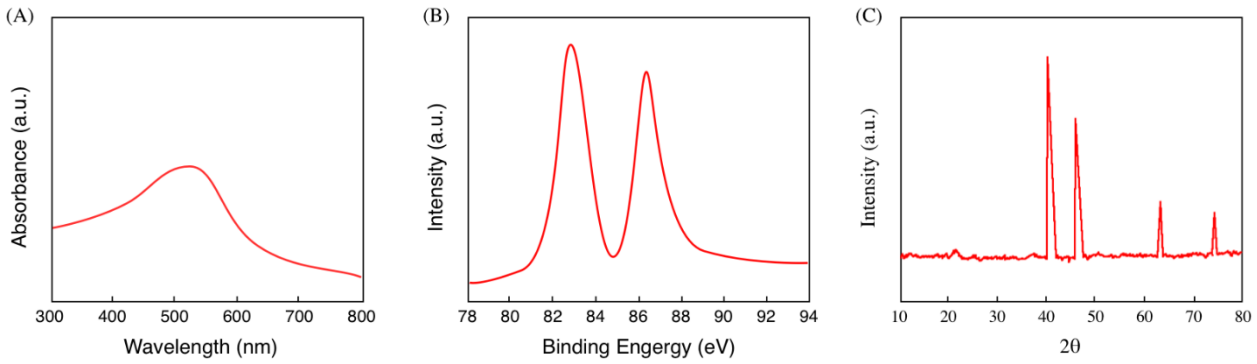

Figure 1. (A) UV-vis spectrum of biosynthesized Au nanoparticles, (B) High resolution Au 4f XPD scan of biosynthesized Au nanoparticles. (C) XRD profile of the biosynthesized Au nanoparticles.

The ATR (attenuated total reflection) mode was tuned for the characterization of APTES/ITO Au(MPA)/APTES/ITO and Au-CK/Au(MPA)/APTES/ITO, as indicated through their FTIR spectra in Figure 2. The 1053 cm^{-1} band, characteristic of Si–O–Si, is present for the APTES. The C=O

stretching vibrations in the MPA-functionalized Au NP carboxylic species accounts for the peak at 1745 cm^{-1}. The –OH stretching and bending vibrations of the carboxylic acid species are apparent from the 2964 and 931 cm^{-1} peaks. N–H stretching and bending vibrations could be, respectively, described by the extra 3387 and 1611 cm^{-1} peaks after the Ab-CK was immobilized. The generation of the amide bond between Ab-CK molecules and Au(MPA) nanoparticles is supported by the above results.

The capacity of measuring the property of monolayer films is a remarkable advantage of Cyclic voltammetry. These films would impede the shift reactions at the interface of electrolyte and the electrode modified by APTES. Note that in this blocking mechanism, a redox couple was employed as a probe molecule. The peak-to-peak potential separation (ΔEp) was about 50 mV at and the ratio of the redox peak current *Ipa*/*Ipc* was about 1 suggesting that the electrochemical reaction is reversible as a result of the construction of the AuNPs and the small peak-to-peak separation indicated a fast electron transfer rate [24, 25]. EIS is an efficient instrumental technique capable of quantitatively and qualitatively characterizing the electrochemical courses at the interface of an electrode and a solution (modified electrodes), and is regarded as a major method of immunosensor behaviour evaluation. The response of the this system after AC signal with insignificant amplitude at diverse frequencies is observed via EIS. Data regarding significant reaction rates can be gathered at the interface of electrode/solution, though chemical bonds or intermediates identification cannot be achieved via this method.

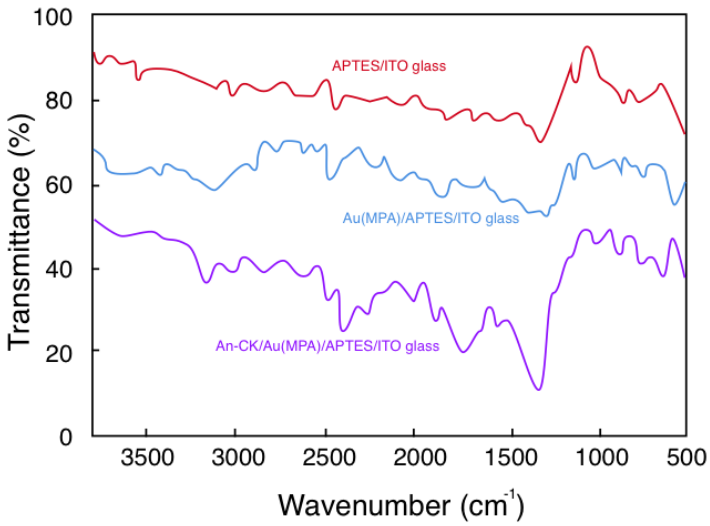

Figure 2. FTIR spectra of APTES/ITO-glass Au(MPA)/APTES/ITO-glass and Ab-CK/Au(MPA)/APTES/ITO-glass.

EIS is usually performed using an 'equivalent circuit' comprised of an assembly of electrical circuit elements that model the physicoelectric characteristics of the electrode/solution interface. The Randles equivalent circuit model fitted to the experiment was adopted in this study, with its components of R_s, Z_w, C_{dl} and R_{et}, respectively, representing (i) ohmic resistance of the electrolyte solution, (ii) Warburg impedance, (iii) interfacial double layer capacitance between a solution and an

electrode and (iv) electron-transfer resistance. The second one is attributed to ion diffusion from bulk electrolyte into the interface of the electrode, and the third one is associated with the electrode surface condition. Replacing the classical capacitance with a constant phase element (CPE) contributes to the modification of the equivalent circuit model; thus, surface heterogeneity or roughness of the electrode could be incorporated with Helmholtz double layer. The real component of impedance (Z′) generally indicates electron transfer resistance (R_{et}) which has been observed to be favorable than capacitive changes. Moreover, the responses of the antibody–antigen interaction are most desirably reflected by the real component of impedance (Z′) in sensitiveness and directness. Despite the possible similar performance of the imaginary component (−Z″) (not shown), this work employed the real component of the impedance as the sensor signal to recognize analyte [26]. CPE is also arranged parallel to Z_w and R_{et}. In addition, the three circuits are arranged in series with R_s. The CPE associated impedance is presented in the equation as follows:

$$Z_{CPE}(\omega) = 1/Y_0(j\omega)^n$$

Herein Y_0, j, ω, and n respectively represent a constant, an imaginary number, the angular frequency and CPE exponent. Taking the role of the heterogeneity gauge, the last one provides detailed information concerning the degree of surface inhomogeneity. The value of n is determinative of CPE which could stand for resistance, capacitance (n = 1, Y_0 = C), inductance (n = −1) or Warburg element (n = 0.5). That minimum defects exist in modification layer on the surface of electrode is reflected through the value of the exponent n of approximately 1, which also reveals the resemblance of CPE to a pseudo capacitor in this work. Diverse designed electrodes have their impedance performance characterized via Z' *vs.* $-Z''$ in Nyquist plots, respectively, standing for the real component and imaginary component of the impedance. A (i) high frequency semicircle and (ii) lower frequency straight area are characteristically shown in the plots. Non-Faradaic impedance biosensors perform impedance measurement in the absence of any redox probe. Bacteria detection is based on the impedance change upon the attachment of bacterial cells on an interdigitated microelectrode in the absence of any redox probe in the sample solution [27]. The first one represents the Faradaic electron transport course where the diameter of the semicircle is equivalent to R_{et}, while the diffusion-limited redox groups' transfer from electrolyte to electrode interface is characterized by the second one. Proper results can be provided by the opted fitting circuit model, which was indicated by the insignificant χ^2 values of the order of 10^{-4}. Diverse designed electrodes are characterized with equivalent circuits, as indicated in the insets (Figure 3). The R_{et} value of 22.55 Ω cm^2 for APTES/ITO-glass is substantially lower than the R_{et} value of 82.60 Ω cm^2 for the original ITO-glass, revealing a simple electron transfer at the interface of the electrode surface. The protonation (NH_3^+) of the APTES amino species in the aqueous solution leads to the significant affinity of the anionic probe $[Fe(CN)_6]^{3-/4-}$ to the polycationic layer, thus its concentration rises at the interface of electrode/solution, and consequently the value of R_{et} declines with a relatively elevated Y_0 value (4.77 μF/cm)., After Au(MPA)-NPs are attached covalently to the silane layer, there is a decline in Y_0 to 3.08 μF/cm^2, as well as a substantial rise in R_{et} to 107.5 Ωcm2 presumably due to the charge repulsion associated with the negatively charged Au(MPA)-NP carboxyl species (pH 7.4) and the anionic probe at the interface of the electrode/solution. To explore this idea further, EIS was conducted on APTES/ITO-glass electrode

modified by a non-carboxyl-functionalized Au NPs in the absence of MPA capping. The unbound electrons transport from the probe to the surface of the electrode is revealed from the substantial R_{et} decline to 9.0 Ω cm^2. This variation coincides with the decline in the semicircle diameter, as revealed in the Nyquist plot. The large amount of unbound carboxyl species on the Au/(MPA)/APTES/ITO-glass electrode surface is confirmed by the utmost significant relative signal variation in terms of the Au(MPA)-NP-modified electrode in comparison with the Au NP-modified electrode. Moreover, Y_0 declining to 2.36 μF/cm^2 and the value of R_{et} increasing to 188.1 Ω cm^2 (in a remarkable degree) occurred presumably because the antibody of cardiac myoglobin protein is covalently immobilized on the Au(MPA) NPs over the surface of the electrode, and BSA blocks non-specific binding sites. The data support the idea that the protein molecule is functioning as insulation, impeding the probe in its mass and charge transport to the surface of the electrode.

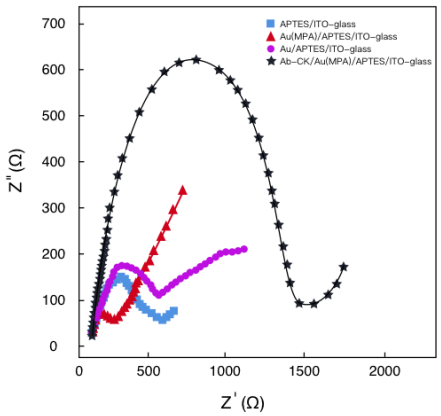

Figure 3. Nyquist plots determined for the original ITO glass plate; APTES/ITO-glass; Au(MPA)/APTES/ITO-glass; Au/APTES/ITO-glass and Ab-CK/Au(MPA)/APTES/ITO-glass in 2 mM $[Fe(CN)_6]^{3-/4-}$ with 0.1 M KCl (voltage: 0.05 V; Frequency range: 1 Hz - 100 kHz.).

An antibody–antigen complex is generated since Ab-CK specifically immunoreacts with the target of Ag-CK on the surface of the electrode. Herein, the latter is complementary to the former. The interfacial electrons at the interface of bioelectrode/solution are prevented from transferring electrons, due to the kinetic barrier created by the generation of the immunocomplex. There is an increase in electron transport resistance and a corresponding decline in capacitance with the increased hindrance of a redox couple's Faradaic reaction. The control specimen was set as the specimen solution in the absence of the target protein of Ag-CK, with the related R_{et} value as the response of the control specimen. Nyquist plots determined succeeding the continuous addition of equal target protein antigen portions with diverse concentration are shown in Figure 4. The interaction between antibody and antigen causes the added Ag-CK to rise in concentration, thus leading to a significant rise in Nyquist circles' diameter, as indicated in the plots. The bioelectrode was found to decline in its capacitive performance due to the immunoreactions, as suggested by an insignificant but observable decline in Y_0.

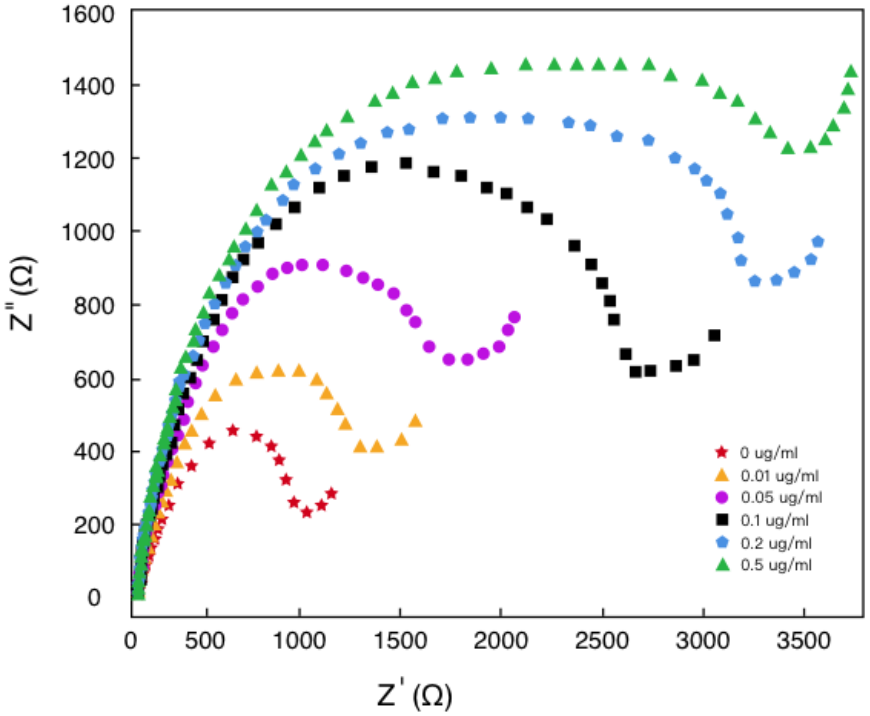

Figure 4. Faradaic impedance spectra of the Ab-CK/Au(MPA)/APTES/ITO-glass electrode preceding and succeeding incubation with diverse concentrations of Ag-CK in PBS (pH 7.4) with 0.1 M KCl solution containing 2 mM $[Fe(CN)_6]^{3-/4-}$ (voltage: 0.05 V; Frequency range: 1 Hz - 100 kHz).

The variation in specific electron charge transfer resistance (ΔR_{et} = $(R_{et})_{after\ immunoreaction}$ − $(R_{et})_{control}$) *vs.* the logarithmic value of Ag-CK concentration (10 ng/mL - 0.5 μg/mL) was plotted to assess the sensitivity of the as-biosynthesized electrode (Figure 5). Herein, 3.7 ng/mL was determined to be the detection limit, which is triple the ratio of signal-to-noise. In addition, the proposed Ab-CK/Au(MPA)/APTES/ITO-glass electrode was utilized to analyze the CK in serum sample. The results of CK content determination in these serum samples were showed in Table 1. As shown, the Ab-CK/Au(MPA)/APTES/ITO-glass electrode has an excellent performance of CK detection for real samples. Additionally, we have compared this electrode with some other modified electrodes for the determination of CK, as summarized in Table 2.

Table 1. The contents and recoveries of Ab-CK/Au(MPA)/APTES/ITO-glass electrode for CK determination in serum (n=3).

No.	Added (μg/mL)	Found (μg/mL)	Chromatographic detection (μg/mL)	Recovery (%)	RSD (%)
Serum 1	0.05	0.0487	0.0519	97.40	2.74
Serum 2	0.10	0.1053	0.1047	105.3	3.11

Table 2. CK determination performance comparison between Ab-CK/Au(MPA)/APTES/ITO-glass electrode and other reports.

Detection method	LR (μg/mL)	DL (μg/mL)	Reference
Enzymes catalytic activity concentrations method	0.4-200	0.05	[28]
chromatographic technique	—	0.05	[29]
ELISA	—	0.42	[30]
Ab-CK/Au(MPA)/APTES/ITO-glass	0.01-0.5	0.0037	This work

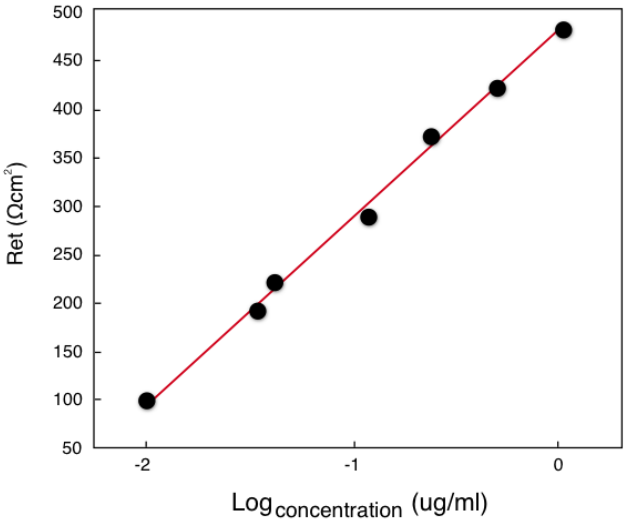

Figure 5. Relationship between logarithm of concentration and Faradaic impedance spectra.

Under no competition circumstances, the selectivity of the sensor was evaluated. Myoglobin (Myo), BSA, troponin T (TnT) and other biological fluids are potential materials for interference, thus they were chosen as the interfering groups to be tested. Concentrations of 50 ng/mL Myo, 50 ng/mL of TnT, together with 100 ng/mL of CK were tested in the non-competition assay. The concentration levels of cardiac biomarkers which are typically present in the serum during ischaemic heart episodes are employed for this experiment. The peak current in terms of Myo varied by +3.1%, while that of TnT by +5.5%. To make sure of desirable reproducibility, triple assays were conducted by means of diverse Au SPE.

4. CONCLUSION

Using *Pithophora oedogonia* as a reducing agent, the Au NPs were synthesized via a designed biosynthesis approach in this study. The concentration of CK was subsequently measured utilizing an

EIS biosensor capable of rapid diagnosis of injuries concerning muscles and AMI. This designed EIS sensor features a linear CK concentration detection in the range of 10 ng/mL to 0.5 μg/mL (with 5.3 ng/mL as the limit of detection).

References

1. C. Liu, L. Jiang, H. Wang, Z. Guo and X. Cai, *Sensors and Actuators B: Chemical*, 122 (2007) 295.
2. G. Davis, M. Green and H. Hill, *Enzyme and microbial technology*, 8 (1986) 349.
3. F. Moreira, R. Dutra, J. Noronha and M. Sales, *Biosensors and Bioelectronics*, 56 (2014) 217.
4. R. Lopes, Y. Lokhnygina, V. Hasselblad, K. Newby, E. Yow, C. Granger, P. Armstrong, J. Hochman, J. Mills and W. Ruzyllo, *Trials*, 14 (2013) 123.
5. R. Mani, O. Herasymowych and C. Kay, *International Journal of Biochemistry*, 11 (1980) 207.
6. V. Glaser, G. Leipnitz, M. Straliotto, J. Oliveira, V. dos Santos, C. Wannmacher, A. de Bem, J.B.T. Rocha, M. Farina and A. Latini, *Neurotoxicology*, 31 (2010) 454.
7. T. Hoshino, Y. Sakai, K. Yamashita, Y. Shirahase, K. Sakaguchi, A. Asaeda, K. Kishi, U. Schlattner, T. Wallimann and M. Yanai, *Scandinavian Journal of Clinical and Laboratory Investigation*, 69 (2009) 687.
8. T. Toyoda, S. Kuan and G. Guilbault, *Anal. Chem.*, 57 (1985) 2346.
9. T. Costa, C. Strunz, J. Nicolau and P. Gutierrez, *The American Journal of Cardiology*, 101 (2008) 311.
10. T. Kurihara, A. Yanagida, H. Yokoi, A. Koyata, T. Matsuya, J. Ogawa, Y. Okamura and D. Miyamoto, *Analytical Biochemistry*, 375 (2008) 144.
11. K. Lo, S. Hurst, K. Atkinson, T. Vandenbogaerde, C. Beaven and J. Ingram, *Journal of Science and Medicine in Sport*, 13 (2010) 117.
12. J. Vidal, J. Bertolín, L. Bonel, L. Asturias, M. Arcos-Martínez and J. Castillo, *Journal of Pharmaceutical and Biomedical Analysis*, 125 (2016) 54.
13. V. Lattanzio, B. Ciasca, S. Powers and C. von Holst, *TrAC Trends in Analytical Chemistry*, 76 (2016) 137.
14. G. Liu and C. Chai, *Analytical Methods*, 7 (2015) 1572.
15. Q. Fang, L. Wang, Q. Cheng, Y. Wang, S. Wang, J. Cai and F. Liu, *Food Anal. Methods*, 8 (2015) 1248.
16. L. Du, W. Ji, Y. Zhang, C. Zhang, G. Liu and S. Wang, *The Analyst*, 140 (2015) 2001.
17. Q. Yu, H. Li, C. Li, S. Zhang, J. Shen and Z. Wang, *Food Control*, 54 (2015) 347.
18. C. Song, C. Liu, S. Wu, H. Li, H. Guo, B. Yang, S. Qiu, J. Li, L. Liu and H. Zeng, *Food Control*, 59 (2016) 345.
19. J. Zhang, P. Shi, P. Yan, M. Wang, Q. Tang, A. Deng and J. Li, *Journal of The Electrochemical Society*, 162 (2015) B22.
20. N. Khunrattanaporn, P. Rijiravanich, M. Somasundrum and W. Surareungchai, *Biosensors and Bioelectronics*, 73 (2015) 181.
21. Z. Farka, T. Juřík, M. Pastucha, D. Kovář, K. Lacina and P. Skládal, *Electroanalysis*, 28 (2016) 1803.
22. L. Yu, Y. Zhang, C. Hu, H. Wu, Y. Yang, C. Huang and N. Jia, *Food Chemistry*, 176 (2015) 22.
23. V. Vilas, D. Philip and J. Mathew, *Journal of Molecular Liquids*, 221 (2016) 179.
24. S. Pakapongpan, R. Palangsuntikul and W. Surareungchai, *Electrochimica Acta*, 56 (2011) 6831.
25. Y. Lin and P. Peng, *Anal. Chim. Acta.*, 869 (2015) 34.
26. Y. Lin, J. Luo, C. Chiou, C. Yang, C. Wang, C. Chou and C. Lai, *Sensors and Actuators B: Chemical*, 186 (2013) 374.
27. S. Radke and E. Alocilja, *Biosensors & bioelectronics*, 20 (2005) 1662.
28. M. Waldron, K. Whelan, O. Jeffries, D. Burt, L. Howe and S.D. Patterson, *Applied Physiology,*

Nutrition, and Metabolism, (2017) 1.
29. C. Smith, L. Bernstein, R. Davis, D. Rind and R. Shmerling, *Archives of Internal Medicine*, 163 (2003) 688.
30. M. Levy, D. Heels-Ansdell, R. Hiralal, M. Bhandari, G. Guyatt, S. Yusuf, D. Cook, J. Villar, M. McQueen and E. McFalls, *The Journal of the American Society of Anesthesiologists*, 114 (2011) 796.